AIMS Mathematics, 8(6): 14142–14166.
DOI: 10.3934/math.2023723
Received: 10 January 2023
Revised: 07 March 2023
Accepted: 17 March 2023
Published: 17 April 2023

http://www.aimspress.com/journal/Math

Research article

Modeling the role of public health intervention measures in halting the transmission of monkeypox virus

Rubayyi T. Alqahtani[1], **Salihu S. Musa**[2,3,4,*] **and Mustafa Inc**[5,6,*]

[1] Department of Mathematics and Statistics, Imam Mohammad Ibn Saud Islamic University, Riyadh 11564, Saudi Arabia
[2] Department of Applied Mathematics, Hong Kong Polytechnic University, Hong Kong SAR, China
[3] Department of Mathematics, Kano University of Science and Technology, Wudil, Kano, Nigeria
[4] Operational Research Center in Healthcare, Near East University TRNC, Nicosia 99138, Turkey
[5] Department of Mathematics, Firat University, Elazig 23119, Turkey
[6] Department of Medical Research, China Medical University, Taichung 40402, Taiwan

* **Correspondence:** salihu-sabiu.musa@connect.polyu.hk, minc@firat.edu.tr.

Abstract: Monkeypox (mpox), a zoonotic viral disease caused by the monkeypox virus (mpoxv), is endemic in many countries in West Africa and is sometimes exported to other parts of the world. The recent outbreak of mpoxv in humans, in endemic and non-endemic countries, has created substantial public health concern worldwide. This research uses a mechanistic model to study the transmission dynamics of mpoxv epidemics in the USA. Our model describes the interaction between different categories of individuals represent various infection phases and hospitalization processes. The model also takes into account the extent of compliance with non-pharmaceutical intervention strategies (NPIs), such as using condoms during sexual contact, quarantine and avoiding large gatherings. The model's equilibria are analyzed, and results on asymptotic stability are obtained. Moreover, the basic reproductive number and other threshold quantities are used to establish the conditions for a forward or backward bifurcation. Our model accurately captures the incidence curves from mpox surveillance data for the USA, indicating that it can be used to explain mpoxv transmission and suggest some effective ways to enhance control efforts. In addition, numerical simulations are carried out to examine the influence of some parameters on the overall dynamics of the model. A partial rank correlation coefficient is adopted for the sensitivity analysis to determine the model most important parameters, which require close attention for effective mpoxv prevention and control. We conclude that it is especially important to ensure that NPIs are properly followed to mitigate mpoxv outbreaks effectively.

Keywords: monkeypox; epidemic; epidemic model; reproduction number; stability analysis
Mathematics Subject Classification: 34A34, 34C23

1. Introduction

The outbreak of the monkeypox virus (mpoxv) across numerous non-endemic countries since May 2022 shows some distint clinical and epidemiological features from previous mpoxv outbreaks, most notably its discerned development and dominance amongst men who have sex with men (MSM) or those who identify as gay or bisexual [14]. The majority of recent mpoxv cases have no history of travel to endemic regions or proven contact with infected animals [14]. The geographic dispersion and rapid increase in cases indicate substantial person-to-person transmission rather than infection from an animal reservoir [14]. Additionally, this is the first significant outbreak of mpoxv that is MSM-dominated and has a significant sexually associated transmission route [14, 34]. It has also been discovered in Nigeria that mpoxv is likely more predominant in young males and is also linked to genital lesions [14, 21, 35].

By March 2023, more than 86,000 people have been infected with mpoxv worldwide, among which more than 98% of infections have occurred in places that have not experienced transmission of this disease before. Over 100 people have died since the large outbreak of mpoxv in May 2022 [7]. In the USA, there have been over 30,000 cases (with 38 death cases), with the largest number of infections since the beginning of the large epidemics in 2022 [8]. The majority of those infected are MSM [14].

Mpox, a disease caused by mpoxv, spreads from person to person through close contact with respiratory secretions or skin sores from an infected individual [47]. Transmission via respiratory droplets requires prolonged face-to-face contact [47], which makes healthcare professionals, household members, and other close contacts of active cases especially vulnerable [47]. The longest documented chain of transmission has increased from 6 to 9 person-to-person infections. This could be attributed to a general decline in immunity due to the cessation of smallpox vaccination. Transmission can also occur from mother to fetus via the placenta or during close contact during or after birth [47]. The extent to which mpox can be transmitted via sexual contact is still unclear. More research is required to understand this risk fully. Mpoxv is a zoonotic virus that spreads to humans by direct contact with infected animals' blood, body fluids, or cutaneous or mucosal lesions [47]. The disease has an incubation period of two to four weeks [14, 21, 47].

A considerable number of epidemic models have been developed and employed to understand mpoxv transmission; see, for instance, [4, 12, 14, 21, 29, 34–38, 46, 51–53] and the references therein. In particular, Yuan et al. [51] analyzed the transmission dynamics of mpoxv in metropolitan municipalities. Vaccination was incorporated into the model to examine its impact on mpoxv transmission at large gatherings [52]. In addition, Endo et al. [14] fitted a dynamic model to empirical sexual partnership and mpox data and revealed that the heavy-tailed sexual partnership distribution could be used to explain the expansion of current mpoxv outbreaks, especially among MSM. An SIR-based model was used by Peter et al. [36] to explore the transmission behavior of mpox. The model was extended by incorporating a fractional order approach [37] to gain more detailed insight into mpoxv transmission. Ward et al. [46] also used a statistical modelling framework taken advantage of contact tracing data to investigate the mpoxv dynamics in the UK. Their results suggested that the mpoxv epidemic peaked in the UK in early July and began to decline afterward. A similar technique was implemented by Musa et al. [29] to investigate the time-varying reproduction number of mpoxv in Nigeria. They found that mpoxv transmission reached an all-time peak in 2022.

Zumla et al. [56] investigated the dynamics of mpoxv transmission outside of endemic areas. They

emphasized that effective control of mpoxv requires preventing widespread infection among frontline healthcare workers and the most vulnerable populations. Using a multi-group dynamic model, Yang et al. [49] examined the potential for mpox viral transmission from high-risk groups to the general population. They calculated the effective reproduction number (R_{eff}) to be larger than 3, indicating that mpoxv is highly transmissible in MSM and that exposure to high-risk individuals must be minimized. They indicated that prevention of community transmission is vital to curb the spread of mpoxv. In a cross-sectional study, Hernaez et al. [22] discovered high viral loads in the saliva of most mpox patients using quantitative polymerase chain reaction (PCR), and found that they were associated with the severity of skin lesions and symptoms of systemic disease. To remove mpoxv particles from aerosols that can travel a long distance in the air, new nanofiber filters have been developed [22]. Following the discovery of highly viable viral loads in saliva in most mpox patients and mpoxv DNA in droplets and aerosols, the authors concluded that additional epidemiological studies are required to determine whether respiratory route of infection is relevant to the mpoxv outbreak in 2022. Americo et al. [3] studied the virulence variations of mpoxv clades I, IIa, and IIb in a small animal model. They discovered that the clades in the order clade I > clade IIa > clade IIb in CAST/EiJ mice exhibit highly significant differences compared to the severity of clinical disease in humans.

Due to the sizable mpoxv outbreaks in non-endemic communities, recommendations from researchers and public health professionals are urgently required to help identify the primary factors causing the outbreaks and to formulate policies for effective control.

Epidemiological modeling has been used widely to study the transmission dynamics of reemerging diseases [1, 2, 13, 15, 17, 19, 20, 24]. To better comprehend the factors behind the recent rapid spread of mpoxv, we used a dynamic model in this work to imitate the mpoxv outbreaks and analyze the transmission behaviour. The model extends earlier ones (such as [37]) by taking into account several stages of transmission, such as different infection phases, hospitalization, and individuals who do (or do not) adhere to non-pharmaceutical intervention measures (NPIs).

The remainder of this work is organized as follows. In Section 2, an epidemic model is presented. The model is theoretically analyzed in Section 3. We give numerical results in Section 4, and end the paper with a brief discussion and conclusions in Section 5.

2. Materials and methods

2.1. Epidemic data

We retrieved the daily epidemiological cases data of the mpoxv epidemic for the USA, as reported by the Centers for Disease Control Prevention (CDC) [7, 8] from May 10 through December 14, 2022, following laboratory confirmation and case definition of mpoxv. We used the data to calculate the daily cumulative incidence and examined several mpoxv incidence scenarios for the USA.

2.2. Epidemic model

This study uses a traditional SEIR-based model to examine the transmission dynamics and evaluate control measures for the mpoxv epidemic. It describes the epidemiological dynamics of mpoxv transmission. To more accurately analyze the transmission behavior of mpoxv, the proposed model accounts for both those who adhere to and do not adhere to NPI measures. The model explicitly

distinguishes between the various susceptible and infectious stages to assess the overall transmission dynamics of mpoxv outbreaks. The parameter ρ represents the fraction of newly recruited individuals who comply with NPI measures, while $1-\rho$ represents those who do not comply. The model also considers isolation, which is a critical intervention strategy in mpox prevention and control. Several modeling studies have investigated the impact of isolation in suppressing disease transmission (in which infected people are taken into hospitals or isolation centers to prevent large community outbreaks); see, for example, [32, 40], and the references therein.

Our model has the following notable features: (i) We only consider direct or human-to-human transmission routes since we aimed to access the mpoxv transmission dynamics in the USA, which has the highest cases since the re-emergence of mpox on May 2022. (ii) Rodent populations are not incorporated into the model since it is believed that the mpoxv infections in the USA are due to human-to-human transmission. However, the situation is different from sub-Saharan Africa, where mpoxv is endemic, and most of the transmission is zoonotic (i.e., animal-to-human transmission). (iii) Our model extends earlier ones (such as [37, 53]) by taking into account several stages of transmission, such as different infection phases and hospitalization, as well as individuals who adhere (or do not adhere) to basic NPIs (described as high-risk and low-risk populations) to gain a better insight into the overall mpoxv transmission dynamics in the USA and beyond.

We separate the total population of humans at time t, denoted by $N(t)$, into susceptible persons who do not comply with NPIs, $S_n(t)$; susceptible persons who comply with NPIs, $S_y(t)$; exposed persons, $E(t)$; infectious persons who do not comply with NPIs, $I_n(t)$; infectious persons who comply with NPIs, $I_y(t)$; isolated persons, $J(t)$; and recovered persons, $R(t)$, so that $N(t) = S_n(t) + S_y(t) + E(t) + I_n(t) + I_y(t) + J(t) + R(t)$.

Figure 1 shows an overview of the mpoxv model and Table 1 lists the state variables and parameters, which satisfy the following system of nonlinear ordinary differential equations:

$$\begin{aligned}
\frac{\mathrm{d}S_n}{\mathrm{d}t} &= (1-\rho)\pi - \lambda S_n - (\theta+\mu)S_n,\\
\frac{\mathrm{d}S_y}{\mathrm{d}t} &= \rho\pi + \theta S_n - \epsilon\lambda S_y - \mu S_y,\\
\frac{\mathrm{d}E}{\mathrm{d}t} &= \lambda(S_n + \epsilon S_y) - (\sigma_n + \sigma_y + \mu)E,\\
\frac{\mathrm{d}I_n}{\mathrm{d}t} &= \sigma_n E - (\eta + \gamma_n + \tau_n + \delta_n + \mu)I_n,\\
\frac{\mathrm{d}I_y}{\mathrm{d}t} &= \sigma_y E + \eta I_n - (\gamma_y + \tau_y + \delta_y + \mu)I_y,\\
\frac{\mathrm{d}J}{\mathrm{d}t} &= \gamma_n I_n + \gamma_y I_y - (\tau_J + \delta_J + \mu)J,\\
\frac{\mathrm{d}R}{\mathrm{d}t} &= \tau_n I_n + \tau_y I_y + \tau_J J - \mu R.
\end{aligned} \tag{1}$$

The model's force of infection is formulated as follows:

$$\lambda = \frac{\beta(I_n + \alpha I_y)}{N}. \tag{2}$$

Note that $0 < \alpha < 1$ and $0 < \epsilon < 1$ represent alteration parameters for the reduction of infectiousness and efficacy for compliance of NPIs, respectively.

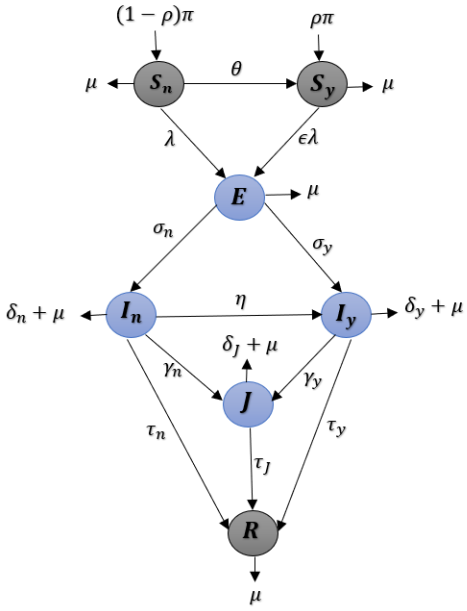

Figure 1. Schematic representation of mpoxv transmission model (1).

Table 1. Explanation of model's variables and parameters.

Variable	**Description**
N	Total humans population
S_n	Susceptible individuals who do not comply with NPIs
S_y	Susceptible individuals who comply with NPIs
E	Exposed individuals
I_n	Symptomatically infectious individuals who do not comply with NPIs
I_y	Symptomatically infectious individuals who do comply with NPIs
J	Isolated individuals
R	Recovered individuals
parameter	
π	Recruitment rate
ρ	Fraction of newly recruited persons to a class of individuals who comply with NPIs measures
μ	Natural death rate
β	Transmission/contact rate
α	Modification parameter for the reduction of infectiousness
θ	Rate of NPIs compliance from S_n to S_y
ϵ	Efficacy of NPIs compliance in preventing mpoxv infection
σ_n, σ_y	Progression rates
η	Rate of NPIs compliance from I_n to I_y
γ_n, γ_y	Isolation/hospitalization rates
τ_n, τ_y, τ_J	Recovery rates
δ_n, δ_y, δ_J	Mpoxv induced death rates

2.3. Basic epidemiological characteristics of the model

Since the model (1) examines the dynamics of mpoxv infection in humans, all of its state variables and parameters are presumptively positive. To study the fundamental analytic characteristics of model (1), we must first take into account the rate of change of the entire human population, N ($N'(t)$, the prime here denotes the derivative with respect to time), which is calculated as follows.

$$\frac{dN}{dt} = \pi - \mu N - \delta_n I_n - \delta_y I_y - \delta_J I_J \leqslant \pi - \mu N. \tag{3}$$

2.3.1. Positivity of model solutions

For the mpoxv model (1) to be biologically reasonable, all state variables must be positive at time $t > 0$. In other words, solutions of model (1) with positive initial data will remain positive for all time $t > 0$.

Lemma 2.1. *Let the initial data* $\Theta(0) \geq 0$*, where* $\Theta(t) = \left(S_n, S_y, E, I_n, I_y, J, R\right)$*. Then the solutions* $\Upsilon(t)$ *of model* (1) *are positive for all* $t > 0$*.*

Proof. Let $t^1 = sup\{t > 0 : \Theta(t) > 0 \in [0, t]\}$. Thus, $t^1 > 0$. Since π and $1 - \rho$ are positive, it follows from the first equation of the model (1) that

$$\frac{dS_n}{dt} \geq -(\lambda(t) + \theta\mu) S_n.$$

Following the comparison theorem in conjunction with the separation of variables method [23, 39, 50], we have

$$S_n(t^1) \geq S_n(0)\exp\left[-\left(\int_0^{t_1} \lambda(u)du + (\theta + \mu)t_1\right)\right] > 0.$$

Hence, $S_n(t) > 0$. Similarly, it can be shown that the remaining components of $\Theta(t)$, i.e., S_y, E, I_n, I_y, J, R are all positive for all $t > 0$. Hence, $\Theta(t) > 0$ for all $t > 0$. □

2.3.2. Invariant region

The following biological feasible region is considered:

$$\Omega = \left\{(S_n, S_y, E, I_n, I_y, J, R) \in \mathbb{R}_+^7 : N \leqslant \frac{\pi}{\mu}\right\}.$$

Since N is positive, to ensure that any solutions of the system that start in the region Ω remain in Ω for all non-negative time t, it is sufficient to look at solutions that are limited to Ω, which is positively-invariant. Therefore, the results for a normal existence, uniqueness, and continuity will be satisfied for model (1) per earlier works [23, 39, 50].

3. Analytical results

3.1. Disease-free equilibrium

Disease-free equilibrium (DFE) of model (1), denoted by Γ^0, is obtained by setting all the equations of the right-hand side of model (1) to zero, that is $\frac{dS_n}{dt} = \frac{dS_y}{dt} = \frac{dE}{dt} = \frac{dI_n}{dt} = \frac{dI_y}{dt} = \frac{dJ}{dt} = \frac{dR}{dt} = 0$. This

yields $S_n^0 = \frac{(1-\rho)\pi}{\theta+\mu}$, $S_y^0 = \frac{\rho\pi+\theta S_n^0}{\mu}$, $E^0 = I_n^0 = I_y^0 = J^* = R^0 = 0$. The DFE for model (1) is given by

$$\Gamma^0 = \{S_n^0, S_y^0, E^0, I_n^0, I_y^0, J^0, R^0\} = \left\{\frac{(1-\rho)\pi}{\theta+\mu}, \frac{\pi(\rho\mu+\theta)}{\mu(\theta+\mu)}, 0, 0, 0, 0, 0\right\}. \tag{4}$$

3.2. Basic reproduction number

Here, we use the next-generation matrix (NGM) method, which was introduced by van den Driessche & Watmough in [45], to calculate model's basic reproduction number $\mathcal{R}_0$, which is the number of secondary cases that a typical primary case would produce in a fully susceptible population during the infectious period [10, 32, 44, 45]. Using the NGM technique, the matrices F, which stands for the new infection terms, and V, which stands for the other transfer terms are calculated and provided below. Note that the linear stability Γ^0 is calculated using (4).

$$\mathcal{F} = \begin{bmatrix} \lambda^0(S_n^0 + \epsilon S_y^0) \\ 0 \\ 0 \\ 0 \end{bmatrix} \quad \text{and} \quad \mathcal{V} = \begin{bmatrix} A_1E^0 \\ -\sigma_n E^0 + A_2 I_n^0 \\ -\sigma_y E^0 - \eta I_n^0 + A_3 I_y^0 \\ -\gamma_n I_n^0 - \gamma_y I_y^0 + A_4 J^0 \end{bmatrix},$$

where $A_1 = \sigma_n+\sigma_y+\mu$, $A_2 = \eta+\gamma_n+\tau_n+\delta_n+\mu$, $A_3 = \gamma_y+\tau_y+\delta_y+\mu$, and $A_4 = \tau_J+\delta_J+\mu$.Consequently, the mpoxv infection and transition matrices are computed as follows:

$$F = \begin{bmatrix} 0 & B_1 & B_2 & 0 \\ 0 & 0 & 0 & 0 \\ 0 & 0 & 0 & 0 \\ 0 & 0 & 0 & 0 \end{bmatrix} \quad \text{and} \quad V = \begin{bmatrix} A_1 & 0 & 0 & 0 \\ -\sigma_n & A_2 & 0 & 0 \\ -\sigma_y & -\eta & A_3 & 0 \\ 0 & -\gamma_n & -\gamma_y & A_4 \end{bmatrix}.$$

Therefore, the $\mathcal{R}_0$ is now computed as

$$\mathcal{R}_0 = \rho(FV^{-1}) = \frac{B_1\sigma_n A_3 + B_2\left(\eta\sigma_n + \sigma_y A_2\right)}{A_1A_2A_3}, \tag{5}$$

with ρ characterising the spectral radius of the NGM, $B_1 = \frac{\beta(S_n^0+\epsilon S_y^0)}{N^0}$, and $B_2 = \frac{\beta\alpha(S_n^0+\epsilon S_y^0)}{N^0}$.

Therefore, based on the Theorem in [45], we established the following results about local stability of the DFE of model (1).

Theorem 3.1. *The DFE of model* (1) *is locally-asymptotically stable whenever* $\mathcal{R}_0 < 1$ *and unstable if* $\mathcal{R}_0 > 1$.

A value $\mathcal{R}_0 < 1$ indicates that a small number of mpoxv cases cannot lead to a large outbreak. For mpoxv containment measures in the epidemic model (1), making $\mathcal{R}_0 < 1$ necessary. Thus, whenever $\mathcal{R}_0 < 1$, mpoxv can be eradicated over time, while mpoxv persistence is continuous for $\mathcal{R}_0 > 1$. Therefore, adequate NPI measures are required to mitigate the disease effectively.

3.3. Endemic equilibrium

When mpoxv infiltrates a community, at least one infected compartment is not empty. Following some algebraic manuplulation, we obtain an endemic equilibrium (EE) state by setting the vector field of the system (1) to zero. Thus, the EE is now given by

$$\Gamma^* = \{S_n^*, S_y^*, E^*, I_n^*, I_y^*, J^*, R^*\}. \tag{6}$$

The following equations give the EE points in terms of λ^*.

$$\begin{aligned}
S_n^{**} &= \frac{(1-\rho)\pi}{\lambda^* + \mu},\\
S_y^{**} &= \frac{\pi\left(((1-\rho))\,\theta + \lambda^*\rho + \mu\rho\right)}{(\epsilon\lambda^* + \mu)(\lambda^* + \mu)},\\
E^{**} &= \frac{\lambda^*\pi\left(((1-\rho))\,\epsilon\lambda^* + ((1-\rho))\,\epsilon\theta + \epsilon\lambda^*\rho + \epsilon\mu\rho + ((1-\rho))\,\mu\right)}{A_1(\lambda^* + \mu)(\epsilon\lambda^* + \mu)},\\
I_n^* &= \frac{\lambda^*\pi\left(((1-\rho))\,\epsilon\lambda^* + ((1-\rho))\,\epsilon\theta + \epsilon\lambda^*\rho + \epsilon\mu\rho + ((1-\rho))\,\mu\right)\sigma_n}{A_1A_2(\lambda^* + \mu)(\epsilon\lambda^* + \mu)},\\
I_y^* &= \frac{\left(\eta\sigma_n + A_2\sigma_y\right)\lambda^*\pi\left(((1-\rho))\,\epsilon\lambda^* + ((1-\rho))\,\epsilon\theta + \epsilon\lambda^*\rho + \epsilon\mu\rho + ((1-\rho))\,\mu\right)}{A_3A_1A_2(\lambda^* + \mu)(\epsilon\lambda^* + \mu)},\\
J^* &= \frac{\left(\eta\gamma_y\sigma_n + A_2\gamma_y\sigma_y + A_3\gamma_n\sigma_n\right)\lambda^*\pi\left(((1-\rho))\,\epsilon\lambda^* + ((1-\rho))\,\epsilon\theta + \epsilon\lambda^*\rho + \epsilon\mu\rho + ((1-\rho))\,\mu\right)}{A_4A_3A_1A_2(\lambda^* + \mu)(\epsilon\lambda^* + \mu)},\\
R^* &= \Big[\frac{\lambda^*\pi\left(((1-\rho))\,\epsilon\lambda^* + ((1-\rho))\,\epsilon\theta + \epsilon\lambda^*\rho + \epsilon\mu\rho + ((1-\rho))\,\mu\right)}{\mu A_4A_3A_1A_2(\lambda^* + \mu)(\epsilon\lambda^* + \mu)}\Big]\\
&\times\left(\eta A_4\sigma_n\tau_y + \eta\gamma_y\sigma_n\tau_J + A_2A_4\sigma_y\tau_y + A_2\gamma_y\sigma_y\tau_J + A_3A_4\sigma_n\tau_n + A_3\gamma_n\sigma_n\tau_J\right).
\end{aligned} \tag{7}$$

Epidemiologically, the existence of the EE state indicates that at least one of the infected classes in the model is not empty, which shows that the mpoxv spreads and persists in the community.

3.4. Stability analysis of the endemic equilibrium

In this section, we examine the model's interior feasible region, which converges to the singular EE, denoted by Γ^* (6), whenever $\mathcal{R}_0 > 1$. The mpoxv will spread and remain in a population at $\Gamma*$. By driving a Lyapunov function for a model, we demonstrate the overall stability of the EE. This method has been used extensively in earlier works [27, 39, 50].

Theorem 3.2. *The EE Γ^* is globally asymptotically stable (GAS) in the region Ω whenever $\mathcal{R}_0 > 1$ under a specific condition (see Appendix A).*

Appendix A contains a proof of the aforementioned Theorem 3.2. In addition, in Appendix B, a bifurcation phenomenon is analyzed to further assess the dynamics of the model with respect to $\mathcal{R}_0$.

4. Numerical results

4.1. Fitting results

We obtained reported mpoxv outbreak data for the USA from the Centers for Disease Prevention and Control (CDC) [8] and fitted the mpoxv model(1) to the data using Pearson's Chi-square test and the least-squares framework, implemented in the R statistical software (version 4.1.1) [23, 54].

In the numerical fitting results, the daily and cumulative numbers of mpoxv cases from May 10, 2022, through December 14, 2022, were used to fit the mpoxv model. As shown in Figure 2, the results revealed that the model (1) fitted the cumulative and the daily number of reported cases of mpoxv well, indicating that the model can be used to explain the transmission behavior of the mpoxv dynamics, since it reproduces the patterns of real data on the mpox situation in the USA. The parameter values used to fit the model are given in Table 2, with $N(0) = 3.35374570 \times 10^8$ million [9, 48], $S_n(0) = 2.5 \times 10^8$, $S_y(0) = 0.8 \times 10^8$, $E = 800$, $I_n(0) = 5$, $I_y(0) = 1$, $J(0) = 0$, $R(0) = 0$.

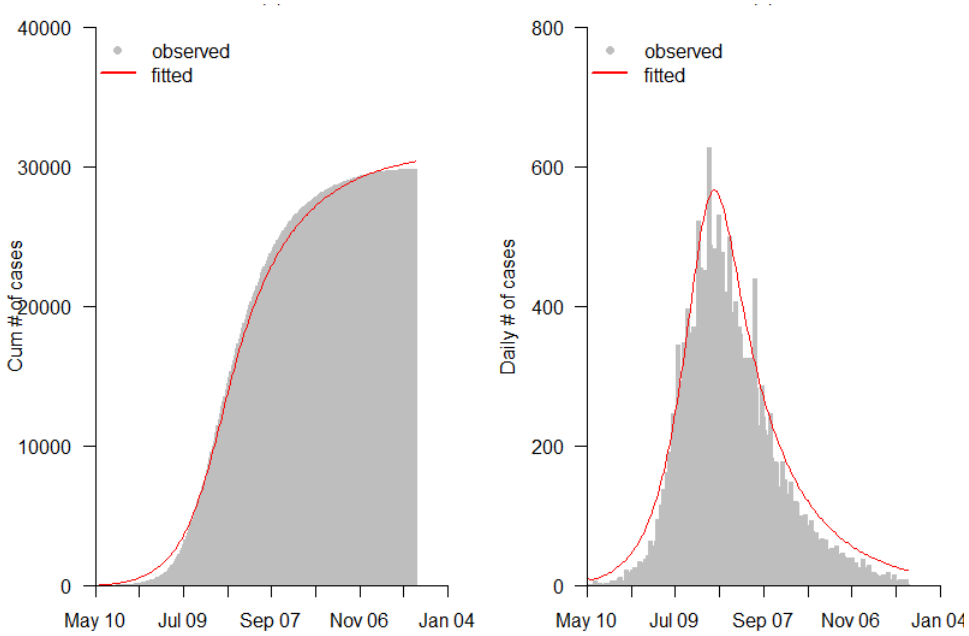

Figure 2. Model fitting results to the cumulative and the daily number of mpoxv cases in the USA for May 10, 2022, through December 14, 2022. In each panel, the grey bars represent the observed number of mpoxv cases, and the red curves are the model-fitting results. The left panel denotes the cumulative number of mpoxv instances, and the right panel shows the daily reported mpoxv cases for the USA for May 10, 2022, through December 14, 2022.

Table 2. Table of parameter values for system (1).

parameter	Baseline (Range)	Units	Sources
N	3.35374570×10^8 (3×10^8 - 3.5×10^8)	persons	[48]
π	12, 074 (10, 000 - 14, 000)	persons per day	[9, 48]
ρ	0.8 (0 - 1)	per day	estimated [25]
μ	3.6×10^{-5} (1.1×10^{-5} - 5.2×10^{-5})	per day	[9, 48]
β	0.1565147 (0.01 - 0.5)	per day	fitted
α	0.75 (0 - 1)	per day	[51]
θ	0.025 (0.01 - 0.75)	per day	estimated [26]
ϵ	0.72 (0 - 1)	per day	assumed
σ_n	0.3204619 (0.21 - 0.87)	per day	fitted
σ_y	0.6729062 (0.21 - 0.87)	per day	fitted
η	0.03486687 (0.01 - 0.05)	per day	fitted
γ_n	0.2 (0.1 - 0.5)	per day	[51]
γ_y	0.04 (0.03 - 0.05)	per day	[51]
τ_n	0.048 (0.001 - 0.075)	per day	[51]
τ_y	0.05 (0.001 - 0.075)	per day	[51]
τ_J	0.056 (0.001 - 0.075)	per day	[51]
δ_n	0.0171 (0.001 - 0.025)	per day	[51]
δ_y	0.0011 (0.001 - 0.025)	per day	[51]
δ_J	0.001 (0.001 - 0.025)	per day	[51]

4.2. Numerical simulations

This section presents various numerical results for the proposed mpoxv model using parameters from Table 2 and different initial conditions for the model's state variables. The model (1) was simulated using the R statistical software to examine its dynamics by varying the values of the transmission rate parameter, which is one of the most crucial parameters in the model and needs to be minimized to control the spread of mpoxv effectively [14, 15, 17, 21, 26, 33, 42, 50]. Figure 3(a)–(d) presents the simulation results. In Figure 3, we used the initial value of β, whereas, in Figure 3(c) and (d), we simulated the model by decreasing the values of β by 25%, 50%, and 75%, respectively, to examine the corresponding dynamics of I_n and I_y in each case.

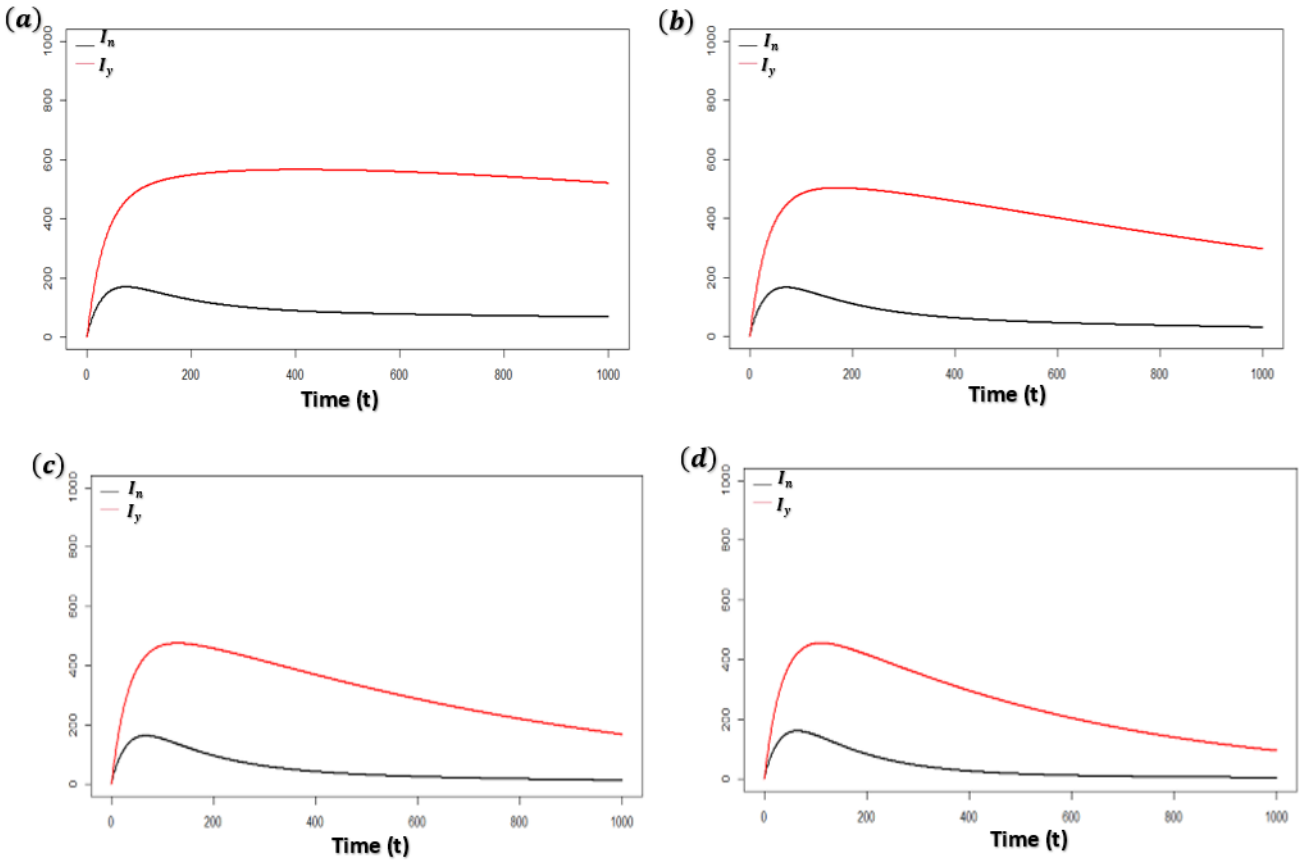

Figure 3. Simulations of the model (1) for I_n and I_y against time (t) with varying transmission rates represented by the panel (a) to (d). The parameter values are given in Table 2 with different initial conditions for the model's state variables.

4.3. Sensitivity analysis

In epidemiological modeling studies, the basic reproduction number $\mathcal{R}_0$ is a crucial parameter that determines whether the disease will continue to spread (persist) or die out in a community when an epidemic occurs [16]. In the current model, we used $\mathcal{R}_0$ and the infection attack rate as response functions to determine the partial rank correlation coefficient (PRCC) for sensitivity analysis to find the most sensitive biological parameters in the model that require maximum attention for mitigation and control [16,32,43,55]. Our sensitivity analysis results show that the parameters β (transmission/contact rate), α_1, and ϵ are the most sensitive, followed by γ_n and τ_y. The PRCC of the basic reproduction number, $\mathcal{R}_0$, and the infection attack rate of the model (1) are presented with the estimated parameters in Figure 4.

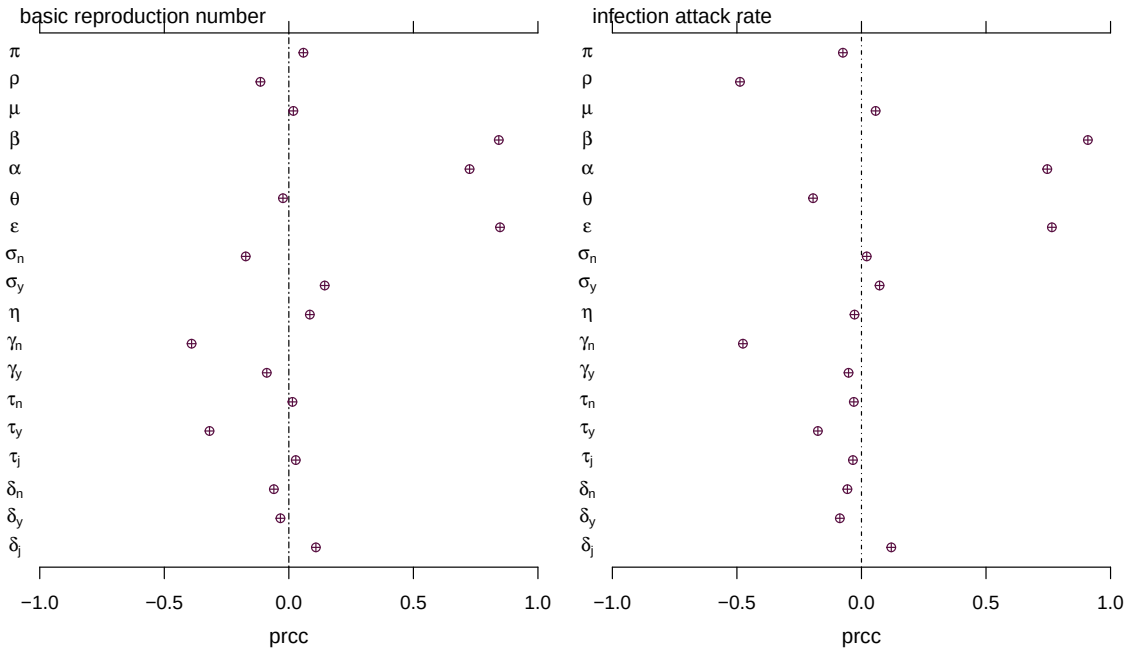

Figure 4. The Partial Rank Correlation Coefficient of *Ro* and the rate of infection attack with respect to the model's parameters. The 95% confidence interval is demonstrated by the bars next to the estimated correlation, shown by the dots. The parameter values utilized for sensitivity analysis are summarized in Table 2.

4.4. Simulations of the global asymptotic stability of the endemic equilibrium

Following the previous approach [17, 33, 39, 42, 50], we provide some numerical examples in this section to demonstrate the global asymptotic stability of the analytical results for the model (1) as provided in the appendix A. All the parameters have the same biological meaning as in Table 2. In Figure 5, we consider the case when the transmission rate parameter $\beta = 0.157$, so that $\mathcal{R}_0$=0.78686606 < 1, while the other parameters have the same values as given in Table 2, with different initial conditions for the model's state variables. The dynamics of the model (1) with $\mathcal{R}_0 < 1$ are presented in Figure 5(a)–(d), which show that the system (1) has an EE, which is GAS whenever $\mathcal{R}_0 < 1$. In Figure 6, we consider the case when the transmission rate parameter $\beta = 0.257$, so that $\mathcal{R}_0 = 1.28805464 > 1$, while the other parameters have the same values as given in Table 2, with different initial conditions for the model's state variables. The dynamics of the model (1) with $\mathcal{R}_0 > 1$ are presented in Figure 6(a)–(d) which show that the system (1) has an EE which is unstable whenever $\mathcal{R}_0 > 1$. These results support the theoretical result stated in Theorem 3.1.

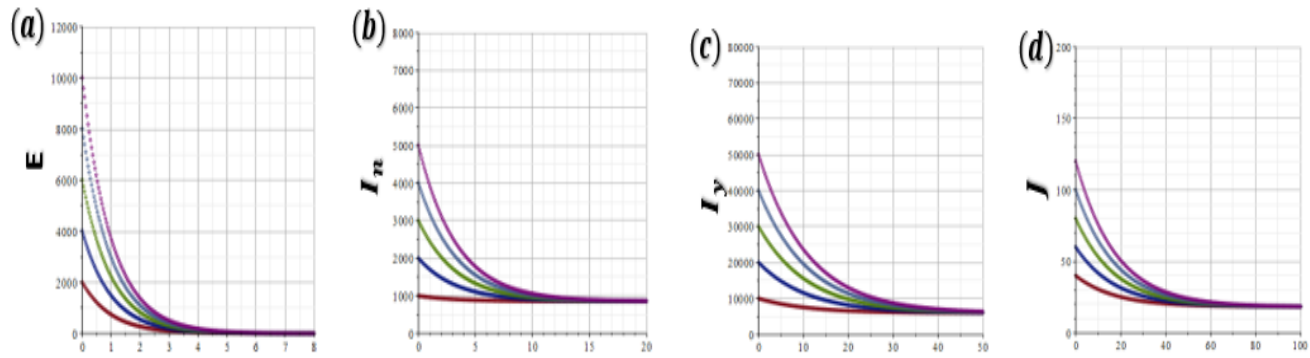

Figure 5. Time series plot of the model (1) with different initial conditions (represented by the different colours). The parameters values are given in Table 2 with $\beta = 0.03$ and $\mathcal{R}_0 < 1$; (a) E, (b) I_n, (c) I_y, (d) J.

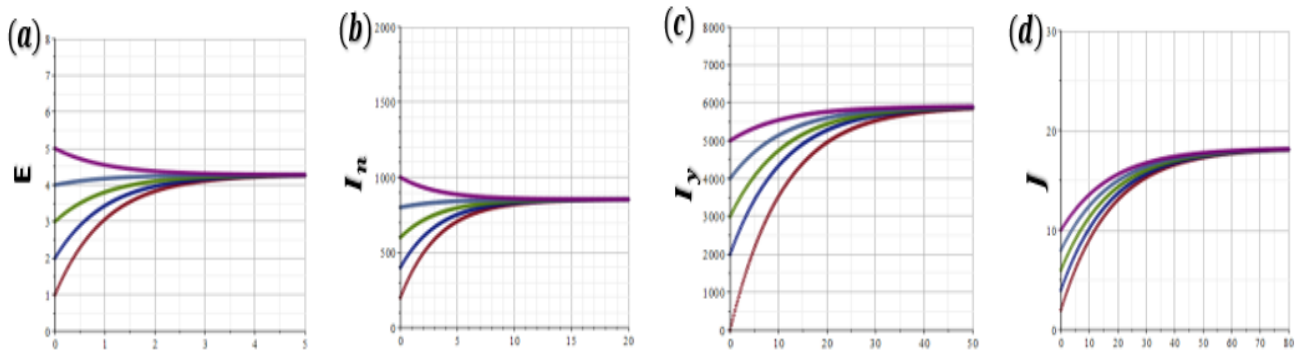

Figure 6. Time series plot of the model (1) with different initial conditions (represented by the different colours). The parameters values are given in Table 2 with $\beta = 0.3$ and $\mathcal{R}_0 > 1$; (a) E, (b) I_n, (c) I_y, (d) J.

5. Discussion and conclusions

Mpox is primarily a zoonotic viral disease that has caused recurrent outbreaks in West Africa and is occasionally transmitted to other regions [47]. It is transmitted to humans through contact with an infected individual or animal, respiratory droplets, or contaminated materials such as bedding [14]. The recent global outbreaks of mpoxv in non-endemic countries have caused substantial public health concern [7]. Although the vaccine used for smallpox is currently in use against mpoxv infection, due to inadequate vaccination levels, the public need to follow basic health precautions to protect themselves and others from mpoxv infection [47].

In this work, we developed a classical SEIR-based model to assess the transmission dynamics of mpoxv epidemics in the USA. The model was fitted successfully to the reported mpoxv cases and

relevant demographic data in the USA. Thus, it can be used to explain the transmission of mpoxv and provide suggestions for optimal control and prevention of the disease. The theoretical and epidemiological outcomes of this work are summarized below.

i) Results on the basic reproduction number of the model were determined analytically and were used to assess the impact of mpoxv control strategies. In addition, subsequent mathematical analysis revealed that the DFE of the model is GAS whenever the $\mathcal{R}_0$ value is below or equal to unity and is unstable when the $\mathcal{R}_0$ is above unity. Further mathematical analysis showed that the EE is GAS whenever $\mathcal{R}_0$ is above unity, indicating the potential for mpoxv to spread and persist in a population. Moreover, we analyzed the forward bifurcation property of the model, which occurs under certain conditions (see Appendix B for more detail). Epidemiologically, the existence of forward bifurcation in the model indicates that the stability of the model exchanges between DFE and EE at $\mathcal{R}_0 = 1$.
   Hence, the stability behavior of the model changes (from stable to unstable) around the endemic equilibrium when the bifurcation parameter β_{hh} changes [11, 17].
ii) The model prediction results provided in Section 4.1 using the daily number of reported mpoxv cases in the USA for the period from May 10 to December 14, 2022, show that the model fitted well to the mpoxv case data, highlighting the applicability of the model to the wave of mpoxv outbreaks.
iii) Numerical results were provided in Section 4.2 to examine the dynamics of the model (1) by decreasing the value of the transmission rate parameter β by 25%, 50%, and 75%, in turn, for each of the variables I_n and I_y. We chose the parameter β since it is one the most crucial parameters in the model and needs to be minimized to effectively control the spread of mpoxv. The results show that the transmission of mpoxv can be significantly reduced if the transmission rate parameter can be decreased as much as possible. This could be achieved if most members of the public complied with NPIs and if governments and other relevant organizations provided adequate medical resources, especially to the most vulnerable communities, to respond to epidemics effectively.
iv) The basic reproduction number and infection attack rates were used as response functions to perform sensitivity analysis of the model (presented in Section 4.3). Partial rank correlation coefficients (PRCC) were used for the sensitivity analysis, which showed that the top three PRCC ranked parameters are the transmission rate, the parameter representing the efficacy of compliance with NPIs in preventing mpoxv infection, and the modification parameter for the reduction of infectiousness. Other parameters with high PRCCs suggesting high priority (although not as high as the top three) include the isolation rate from I_n and recovery rate from I_y. Hence, this study has identified the parameters that should be targeted for effective mpoxv control and prevention.
v) Further numerical results were provided in Section 4.4 to investigate the global stability of the EE for the model (1). The results are illustrated in Figures 5 and 6 and support the theoretical results obtained in 3.2, which revealed that the EE is GAS when $\mathcal{R}_0 > 1$.

In summary, this work employed an SEIR-based model to study and theoretivcally analyze the mpoxv transmission dynamics in the US to shed light on the transmission of mpoxv epidemics, taking into account the roles of NPIs on the overall transmission dynamics. We revealed some vital epidemiological parameters that should be emphasized efforts to mitigate and control of mpoxv. Based on our results, we also observed that the transmission rate and other relevant parameters are

crucial in controlling the spread of mpoxv outbreaks. The results in this paper could play an essential role in developing a long-term plan for controlling mpoxv epidemics, especially for researchers and policymakers. Moreover, our findings could provide an essential reference for policymakers to contain the virus's spread effectively. The model could be extended in the future by incorporating other control vital factors such as pharmaceuticals, human behavior, and seasonality to gain more insight into the transmission of mpoxv.

Acknowledgments

Part of this research was funded and supported by the Deanship of Scientific Research at Imam Mohammad Ibn Saud Islamic University (IMSIU) through Research Partnership Program with number: RP-21-09-07.

Conflict of interest

The authors declare no conflict of interest.

References

1. N. Ahmed, A. Elsonbaty, A. Raza, M. Rafiq, W. Adel, Numerical simulation and stability analysis of a novel reaction-diffusion COVID-19 model, *Nonlinear Dyn.*, **106** (2021), 1293–1310. http://dx.doi.org/10.1007/s11071-021-06623-9
2. N. Ahmed, M. Rafiq, W. Adel, H. Rezazadeh, I. Khan, K. Nisar, Structure preserving numerical analysis of HIV and CD4+ T-cells reaction diffusion model in two space dimensions, *Chaos Soliton. Fract.*, **139** (2020), 110307. http://dx.doi.org/10.1016/j.chaos.2020.110307
3. J. Americo, P. Earl, B. Moss, Virulence differences of mpox (monkeypox) virus clades I, IIa, and IIb. 1 in a small animal model, *PNAS*, **120** (2023), 2220415120. http://dx.doi.org/10.1073/pnas.2220415120
4. S. Bankuru, S. Kossol, W. Hou, P. Mahmoudi, J. Rychtář, D. Taylor, A game-theoretic model of Monkeypox to assess vaccination strategies, *PeerJ*, **8** (2020), 9272. http://dx.doi.org/10.7717/peerj.9272
5. J. Carr, *Applications of centre manifold theory*, New York: Springer, 1981. http://dx.doi.org/10.1007/978-1-4612-5929-9
6. C. Castillo-Chavez, B. Song, Dynamical models of tuberculosis and their applications, *Math. Biosci. Eng.*, **1** (2004), 361–404. http://dx.doi.org/10.3934/mbe.2004.1.361
7. *2022 Mpox outbreak global map*, Centers for Disease Control and Prevention, 2023. Available from: `https://www.cdc.gov/poxvirus/monkeypox/response/2022/world-map.html`
8. *2022 outbreak cases and data*, Centers for Disease Control and Prevention, 2023. Available from: `https://www.cdc.gov/poxvirus/monkeypox/response/2022/index.html`
9. *Life expectancy in the US dropped for the second year in a row in 2021*, Centers for Disease Control and Prevention, 2022. Available from: `https://www.cdc.gov/nchs/pressroom/nchs_press_releases/2022/20220831.htm`

10. O. Diekmann, J. Heesterbeek, J. Metz, On the definition and the computation of the basic reproduction ratio R0 in models for infectious diseases in heterogeneous populations, *J. Math. Biol.*, **28** (1990), 365–382. http://dx.doi.org/10.1007/BF00178324

11. B. Dubey, P. Dubey, U. Dubey, Dynamics of an SIR model with nonlinear incidence and treatment rate, *Appl. Appl. Math.*, **10** (2015), 5.

12. A. El-Mesady, A. Elsonbaty, W. Adel, On nonlinear dynamics of a fractional order monkeypox virus model, *Chaos Soliton. Fract.*, **164** (2022), 112716. http://dx.doi.org/10.1016/j.chaos.2022.112716

13. A. Elsonbaty, Z. Sabir, R. Ramaswamy, W. Adel, Dynamical analysis of a novel discrete fractional SITRS model for COVID-19, *Fractals*, **29** (2021), 2140035. http://dx.doi.org/10.1142/S0218348X21400351

14. A. Endo, H. Murayama, S. Abbott, R. Ratnayake, C. Pearson, W. Edmunds, et al., Heavy-tailed sexual contact networks and monkeypox epidemiology in the global outbreak, *Science*, **378** (2022), 90–94. http://dx.doi.org/10.1126/science.add4507

15. S. Garba, A. Gumel, M. Bakar, Backward bifurcations in dengue transmission dynamics, *Math. Biosci.*, **215** (2008), 11–25. http://dx.doi.org/10.1016/j.mbs.2008.05.002

16. D. Gao, Y. Lou, D. He, T. Porco, Y. Kuang, G. Chowell, et al., Prevention and control of Zika as a mosquito-borne and sexually transmitted disease: a mathematical modeling analysis, *Sci. Rep.*, **6** (2016), 28070. http://dx.doi.org/10.1038/srep28070

17. I. Ghosh, P. Tiwari, J. Chattopadhyay, Effect of active case finding on dengue control: implications from a mathematical model, *J. Theor. Biol.*, **464** (2019), 50–62. http://dx.doi.org/10.1016/j.jtbi.2018.12.027

18. A. Gumel, Causes of backward bifurcations in some epidemiological models, *J. Math. Anal. Appl.*, **395** (2012), 355–365. http://dx.doi.org/10.1016/j.jmaa.2012.04.077

19. H. Gunerhan, H. Rezazadeh, W. Adel, M. Hatami, K. Sagayam, H. Emadifar, et al., Analytical approximate solution of fractional order smoking epidemic model, *Adv. Mech. Eng.*, in press. http://dx.doi.org/10.1177/16878132221123888

20. H. Günerhan, H. Dutta, M. Dokuyucu, W. Adel, Analysis of a fractional HIV model with Caputo and constant proportional Caputo operators, *Chaos Soliton. Fract.*, **139** (2020), 110053. http://dx.doi.org/10.1016/j.chaos.2020.110053

21. C. Happi, I. Adetifa, P. Mbala, R. Njouom, E. Nakoune, A. Happi, et al., Urgent need for a non-discriminatory and non-stigmatizing nomenclature for monkeypox virus, *PLoS Biol.*, **20** (2022), 3001769. http://dx.doi.org/10.1371/journal.pbio.3001769

22. B. Hernaez, A. Muñoz-Gómez, A. Sanchiz, E. Orviz, A. Valls-Carbo, I. Sagastagoitia, et al., Monitoring monkeypox virus in saliva and air samples in Spain: a cross-sectional study, *The Lancet Microbe*, **4** (2023), 21–28. http://dx.doi.org/10.1016/S2666-5247(22)00291-9

23. N. Hussaini, K. Okuneye, A. Gumel, Mathematical analysis of a model for zoonotic visceral leishmaniasis, *Infect. Dis. Model.*, **2** (2017), 455–474. http://dx.doi.org/10.1016/j.idm.2017.12.002

24. M. Izadi, S. Yüzbaşı, W. Adel, Accurate and efficient matrix techniques for solving the fractional Lotka-Volterra population model, *Physica A*, **600** (2022), 127558. http://dx.doi.org/10.1016/j.physa.2022.127558
25. A. Khan, M. Naveed, M. Dur-e-Ahmad, M. Imran, Estimating the basic reproductive ratio for the Ebola outbreak in Liberia and Sierra Leone, *Infect. Dis. Poverty*, **4** (2015), 13. http://dx.doi.org/10.1186/s40249-015-0043-3
26. N. Hussaini, M. Winter, A. Gumel, Qualitative assessment of the role of public health education program on HIV transmission dynamics, *Math. Med. Biol.*, **28** (2011), 245–270. http://dx.doi.org/10.1093/imammb/dqq009
27. J. La Salle, *The stability of dynamical systems*, Philadelphia: SIAM, 1976.
28. Q. Lin, S. Musa, S. Zhao, D. He, Modeling the 2014–2015 Ebola virus disease outbreaks in Sierra Leone, Guinea, and Liberia with effect of high-and low-risk susceptible individuals, *Bull. Math. Biol.*, **82** (2020), 102. http://dx.doi.org/10.1007/s11538-020-00779-y
29. S. Musa, Z. Abdullahi, S. Zhao, U. Bello, N. Hussaini, A. Habib, et al., Transmission dynamics of Monkeypox virus in Nigeria during the current COVID-19 pandemic and estimation of effective reproduction number, *Vaccines*, **10** (2022), 2153. http://dx.doi.org/10.3390/vaccines10122153
30. S. Musa, N. Hussaini, S. Zhao, D. He, Dynamical analysis of chikungunya and dengue co-infection model, *Discrete Cont. Dyn.-B*, **25** (2020), 1907–1933. http://dx.doi.org/10.3934/dcdsb.2020009
31. S. Musa, A. Yusuf, E. Bakare, Z. Abdullahi, L. Adamu, U. Mustapha, et al., Unravelling the dynamics of Lassa fever transmission with differential infectivity: Modeling analysis and control strategies, *Math. Biosci. Eng.*, **19** (2022), 13114–13136. http://dx.doi.org/10.3934/mbe.2022613
32. S. Musa, S. Zhao, D. Gao, Q. Lin, G. Chowell, D. He, Mechanistic modelling of the large-scale Lassa fever epidemics in Nigeria from 2016 to 2019, *J. Theor. Biol.*, **493** (2020), 110209. http://dx.doi.org/10.1016/j.jtbi.2020.110209
33. L. Nkamba, T. Manga, F. Agouanet, M. Mann Manyombe, Mathematical model to assess vaccination and effective contact rate impact in the spread of tuberculosis, *J. Biol. Dyn.*, **13** (2019), 26–42. http://dx.doi.org/10.1080/17513758.2018.1563218
34. D. Ogoina, M. Iroezindu, H. James, R. Oladokun, A. Yinka-Ogunleye, P. Wakama, et al., Clinical course and outcome of human Monkeypox in Nigeria, *Clin. Infect. Dis.*, **71** (2020), 210–214. http://dx.doi.org/10.1093/cid/ciaa143
35. D. Ogoina, J. Izibewule, A. Ogunleye, E. Ederiane, U. Anebonam, A. Neni, et al., The 2017 human monkeypox outbreak in Nigeria-report of outbreak experience and response in the Niger Delta University Teaching Hospital, Bayelsa State, Nigeria, *PLoS. One*, **14** (2019), 0214229. http://dx.doi.org/10.1371/journal.pone.0214229
36. O. Peter, S. Kumar, N. Kumari, F. Oguntolu, K. Oshinubi, R. Musa, Transmission dynamics of Monkeypox virus: a mathematical modelling approach, *Model. Earth Syst. Environ.*, **8** (2022), 3423–3434. http://dx.doi.org/10.1007/s40808-021-01313-2
37. O. Peter, F. Oguntolu, M. Ojo, A. Oyeniyi, R. Jan, I. Khan, Fractional order mathematical model of monkeypox transmission dynamics, *Phys. Scr.*, **97** (2022), 084005. http://dx.doi.org/10.1088/1402-4896/ac7ebc

38. J. Riopelle, V. Munster, J. Port, Atypical and unique transmission of monkeypox virus during the 2022 outbreak: an overview of the current state of knowledge, *Viruses*, **14** (2022), 2012. http://dx.doi.org/10.3390/v14092012

39. P. Roop-O, W. Chinviriyasit, S. Chinviriyasit, The effect of incidence function in backward bifurcation for malaria model with temporary immunity, *Math. Biosci.*, **265** (2015), 47–64. http://dx.doi.org/10.1016/j.mbs.2015.04.008

40. M. Safi, A. Gumel, Qualitative study of a quarantine/isolation model with multiple disease stages, *Appl. Math. Comput.*, **218** (2011), 1941–1961. http://dx.doi.org/10.1016/j.amc.2011.07.007

41. Z. Shuai, P. van den Driessche, Global stability of infectious disease models using Lyapunov functions, *SIAM J. Appl. Math.*, **73** (2013), 1513–1532. http://dx.doi.org/10.1137/120876642

42. G. Sun, J. Xie, S. Huang, Z. Jin, M. Li, L. Liu, Transmission dynamics of cholera: mathematical modeling and control strategies, *Commun. Nonlinear Sci.*, **45** (2017), 235–244. http://dx.doi.org/10.1016/j.cnsns.2016.10.007

43. C. Trotter, N. Gay, W. Edmunds, Dynamic models of meningococcal carriage, disease, and the impact of serogroup C conjugate vaccination. *Am. J. Epidemiol.*, **162** (2005), 89–100. http://dx.doi.org/10.1093/aje/kwi160

44. P. van den Driessche, Reproduction numbers of infectious disease models, *Infectious Disease Modelling* , **2** (2017), 288–303. http://dx.doi.org/10.1016/j.idm.2017.06.002

45. P. van den Driessche, J. Watmough, Reproduction numbers and sub-threshold endemic equilibria for compartmental models of disease transmission, *Math. Biosci.*, **180** (2002), 29–48. http://dx.doi.org/10.1016/S0025-5564(02)00108-6

46. T. Ward, R. Christie, R. Paton, F. Cumming, C. Overton, Transmission dynamics of monkeypox in the United Kingdom: contact tracing study, *BMJ*, **379** (2022), 073153. http://dx.doi.org/10.1136/bmj-2022-073153

47. *Monkeypox*, World Health Organization, 2022. Available from: `https://www.who.int/news-room/fact-sheets/detail/monkeypox?gclid=CjwKCAjws--ZBhAXEiwAv-RNL3T7SFlwhw8Ew8-flekFNnaO9DZaJgz0ybxgg7xwzsIRYi_VAYCb1hoC1OIQAvD_BwE`

48. *Population of the United States (2020 and historical)*, Worldometer, 2022. Available from: `https://www.worldometers.info/world-population/us-population/`.

49. S. Yang, X. Guo, Z. Zhao, B. Abudunaibi, Y. Zhao, J. Rui, et al., Possibility of mpox viral transmission and control from high-risk to the general population: a modeling study, *BMC Infect. Dis.*, **23** (2023), 119. http://dx.doi.org/10.1186/s12879-023-08083-5

50. C. Yang, X. Wang, D. Gao, J. Wang, Impact of awareness programs on cholera dynamics: two modeling approaches, *Bull. Math. Biol.*, **79** (2017), 2109–2131. http://dx.doi.org/10.1007/s11538-017-0322-1

51. P. Yuan, Y. Tan, L. Yang, E. Aruffo, N. Ogden, J. Bélair, et al., Assessing transmission risks and control strategy for monkeypox as an emerging zoonosis in a metropolitan area, *J. Med. Virol.*, **95** (2023), 28137. http://dx.doi.org/10.1002/jmv.28137

52. P. Yuan, Y. Tan, L. Yang, E. Aruffo, N. Ogden, J. Belair, et al., Modelling vaccination and control strategies for outbreaks of monkeypox at gatherings, *Front. Public Health*, **10** (2022), 1026489. http://dx.doi.org/10.3389/fpubh.2022.1026489

53. M. Al-Shomrani, S. Musa, A. Yusuf, Unfolding the transmission dynamics of monkeypox virus: an epidemiological modelling analysis, *Mathematics*, **11** (2023), 1121. http://dx.doi.org/10.3390/math11051121

54. Z. Yuan, S. Musa, S. Hsu, C. Cheung, D. He, Post pandemic fatigue: what are effective strategies? *Sci. Rep.*, **12** (2022), 9706. http://dx.doi.org/10.1038/s41598-022-13597-0

55. S. Zhao, L. Stone, D. Gao, D. He, Modelling the large-scale yellow fever outbreak in Luanda, Angola, and the impact of vaccination, *PLoS Neglect. Trop. Dis.*, **12** (2018), 0006158. http://dx.doi.org/10.1371/journal.pntd.0006158

56. A. Zumla, S. Valdoleiros, N. Haider, D. Asogun, F. Ntoumi, E. Petersen, et al., Monkeypox outbreaks outside endemic regions: scientific and social priorities, *Lancet Infect. Dis.*, **22** (2022), 929–931. http://dx.doi.org/10.1016/S1473-3099(22)00354-1

Appendix A: Proof of global stability analysis

In this section, we prove Theorem 3.2.

Proof. To prove Theorem 3.2, we adopted previous technique [39, 41, 50], and designed a Lyapunov function given below.

$$\begin{aligned}\mathfrak{I}(t) =&\iota_1\Big(S_n - S_n^* - S_n^* \ln\frac{S_n}{S_n^*}\Big) + \iota_2\Big(S_y - S_y^* - S_y^* \ln\frac{S_y}{S_y^*}\Big) + \iota_3\Big(E - E^* - E^* \ln\frac{E}{E^*}\Big)+\\ &\iota_4\Big(I_n - I_n^* - I_n^* \ln\frac{I_n}{I_n^*}\Big) + \iota_5\Big(I_y - I_y^* - I_y^* \ln\frac{I_y}{I_y^*}\Big) + \iota_6\Big(J - J^* - J^* \ln\frac{J}{J^*}\Big).\end{aligned} \tag{A-1}$$

Therefore, the derivative of the Lyapunov function (A-1) calculated along solutions of the model (1) is given by

$$\dot{\mathfrak{I}}(t) =\iota_1\Big(1 - \frac{S_n^*}{S_n}\Big)\dot{S_n} + \iota_2\Big(1 - \frac{S_y^*}{S_y}\Big)\dot{S_y} + \iota_3\Big(1 - \frac{E^*}{E}\Big)\dot{E} + \iota_4\Big(1 - \frac{I_n^*}{I_n}\Big)\dot{I_n} + \iota_5\Big(1 - \frac{I_y^*}{I_y}\Big)\dot{I_y} + \iota_6\Big(1 - \frac{J^*}{J}\Big)\dot{J}. \tag{A-2}$$

By direct computation from Eq (A-2), we have

$$\begin{aligned}\iota_1\Big(1 - \frac{S_n^*}{S_n}\Big)\dot{S_n} &= \iota_1\Big(1 - \frac{S_n^*}{S_n}\Big)\Big(\pi(1-\rho) - \lambda S_n - A_5 S_n\Big)\\ &= \iota_1\Big(1 - \frac{S_n^*}{S_n}\Big)\Big(\lambda^* S_n^* + A_5 S_n^* - \lambda S_n - A_5 S_n\Big)\\ &= \iota_1\lambda^* S_n^*\Big(1 - \frac{S_n^*}{S_n}\Big)\Big(1 - \frac{\lambda S_n}{\lambda^* S_n^*}\Big) - \iota_1 A_5\frac{(S_n - S_n^*)^2}{S_n}\\ &\leq \iota_1\lambda^* S_n^*\Big(1 - \frac{\lambda S_n}{\lambda^* S_n^*} - \frac{S_n^*}{S_n} + \frac{\lambda}{\lambda^*}\Big),\end{aligned} \tag{A-3}$$

and,

$$\begin{aligned}\iota_2\Big(1-\frac{S_y^*}{S_y}\Big)\dot{S}_y &= \iota_2\Big(1-\frac{S_y^*}{S_y}\Big)\Big(\pi\rho+\theta S_n-\epsilon\lambda S_y-\mu_h S_y\Big)\\ &= \iota_2\Big(1-\frac{S_y^*}{S_y}\Big)\Big(\epsilon\lambda^* S_y^*+\mu_h S_y^*-\epsilon\lambda S_y-\mu_h S_y\Big)\\ &= \iota_2\epsilon\lambda^* S_y^*\Big(1-\frac{S_y^*}{S_y}\Big)\Big(1-\frac{\lambda S_y}{\lambda^* S_y^*}\Big)-\iota_2\mu_h\frac{(S_y-S_y^*)^2}{S_y}\\ &\le \iota_2\epsilon\lambda^* S_y^*\Big(1-\frac{\lambda S_y}{\lambda^* S_y^*}-\frac{S_y^*}{S_y}+\frac{\lambda}{\lambda^*}\Big),\end{aligned} \tag{A-4}$$

and,

$$\begin{aligned}\iota_3\Big(1-\frac{E^*}{E}\Big)\dot{E} &= \iota_3\Big(1-\frac{E^*}{E}\Big)\Big(\lambda S_n+\epsilon\lambda S_y-A_1E\Big)\\ &= \iota_3\Big(1-\frac{E^*}{E}\Big)\Big(\lambda S_n+\epsilon\lambda S_y-(\lambda^* S_n^*+\epsilon\lambda^* S_y^*)\frac{E}{E^*}\Big)\\ &= \iota_3\lambda^* S_n^*\Big(1-\frac{E^*}{E}\Big)\Big(\frac{\lambda S_n}{\lambda^* S_n^*}-\frac{E}{E^*}\Big)+\iota_3\epsilon\lambda^* S_y^*\Big(1-\frac{E^*}{E}\Big)\Big(\frac{\lambda S_y}{\lambda^* S_y^*}-\frac{E}{E^*}\Big)\\ &= \iota_3\lambda^* S_n^*\Big(\frac{\lambda S_n}{\lambda^* S_n^*}-\frac{E}{E^*}-\frac{\lambda S_n E^*}{\lambda^* S_n^* E}+1\Big)+\iota_3\epsilon\lambda^* S_y^*\Big(\frac{\lambda S_y}{\lambda^* S_y^*}-\frac{E}{E^*}-\frac{\lambda S_y E^*}{\lambda^* S_y^* E}+1\Big),\end{aligned} \tag{A-5}$$

and,

$$\begin{aligned}\iota_4\Big(1-\frac{I_n^*}{I_n}\Big)\dot{I}_n &= \iota_4\Big(1-\frac{I_n^*}{I_n}\Big)\Big(\sigma_n E-A_2I_n\Big)\\ &= \iota_4\Big(1-\frac{I_n^*}{I_n}\Big)\Big(\sigma_n E-\sigma_n E^*\frac{I_n}{I_n^*}\Big)\\ &= \iota_4\sigma_n E^*\Big(1-\frac{I_n^*}{I_n}\Big)\Big(\frac{E}{E^*}-\frac{I_n}{I_n^*}\Big)\\ &= \iota_4\sigma_n E^*\Big(\frac{E}{E^*}-\frac{I_n}{I_n^*}-\frac{I_n^*E}{I_nE^*}+1\Big),\end{aligned} \tag{A-6}$$

similarly,

$$\iota_5\Big(1-\frac{I_y^*}{I_y}\Big)\dot{I}_y = \quad = \iota_5\sigma_y E^*\Big(\frac{E}{E^*}-\frac{I_y}{I_y^*}-\frac{E^*I_y}{EI_y^*}+1\Big)+\iota_5\eta I_n^*\Big(\frac{I_n}{I_n^*}-\frac{I_y}{I_y^*}-\frac{I_nI_y^*}{I_n^*I_y}+1\Big), \tag{A-7}$$

and,

$$\iota_6\Big(1-\frac{J^*}{J}\Big)\dot{J} = \quad = \iota_6\gamma_n I_n^*\Big(\frac{I_n}{I_n^*}-\frac{J}{J^*}-\frac{I_nJ^*}{I_n^*J}+1\Big)+\iota_6\gamma_y I_y^*\Big(\frac{I_y}{I_y^*}-\frac{J}{J^*}-\frac{I_yJ^*}{I_y^*J}+1\Big), \tag{A-8}$$

Substituting $\iota_1 = \iota_2 = \iota_3 = \iota_5 = \iota_6 = 1$, $\iota_4 = \frac{\lambda^* S_n^* + \epsilon\lambda^* S_y^*}{\sigma_n E^*}$ and Eqs (A-3)–(A-8) into Eq (A-2), we have

$$\begin{aligned}
\dot{\mathfrak{Z}}(t) \leq & \lambda^* S_n^* \Big(2 - \frac{S_n^*}{S_n} - \frac{E}{E^*} - \frac{\lambda S_n E^*}{\lambda^* S_n^* E} + \frac{\lambda}{\lambda^*}\Big) + \\
& \epsilon\lambda^* S_y^* \Big(2 - \frac{S_y^*}{S_y} - \frac{E}{E^*} - \frac{\lambda S_y E^*}{\lambda^* S_y^* E} + \frac{\lambda}{\lambda^*}\Big) + \\
& \lambda^* S_n^* \Big(\frac{E}{E^*} - \frac{I_n}{I_n^*} - \frac{I_n^* E}{I_n E^*} + 1\Big) + \\
& \epsilon\lambda^* S_y^* \Big(\frac{E}{E^*} - \frac{I_n}{I_n^*} - \frac{I_n^* E}{I_n E^*} + 1\Big) + \\
& \sigma_y E^* \Big(\frac{E}{E^*} - \frac{I_y}{I_y^*} - \frac{E I_y^*}{E^* I_y} + 1\Big) + \\
& \eta I_n^* \Big(\frac{I_n}{I_n^*} - \frac{I_y}{I_y^*} - \frac{I_n I_y^*}{I_n^* I_y} + 1\Big) + \\
& \gamma_n I_n^* \Big(\frac{I_n}{I_n^*} - \frac{J}{J^*} - \frac{I_n J^*}{I_n^* J} + 1\Big) + \\
& \gamma_y I_y^* \Big(\frac{I_y}{I_y^*} - \frac{J}{J^*} - \frac{I_y J^*}{I_y^* J} + 1\Big).
\end{aligned} \tag{A-9}$$

Suppose, a function is define as $u(x) = 1 - x + \ln x$, then, if $x > 0$ it leads to $u(x) \leq 0$. Also, if $x = 1$, then $u(x) = 0$. Implies that $x - 1 \geq \ln(x)$ for any $x > 0$ [28, 50]. By using the above definition, direct calculation from Eq (A-8), and conditions (i) and (ii), we have

$$\begin{aligned}
& \Big(2 - \frac{S_n^*}{S_n} - \frac{E}{E^*} - \frac{\lambda S_n E^*}{\lambda^* S_n^* E} + \frac{\lambda}{\lambda^*}\Big) \\
& = \Big(- (1 - \frac{\lambda}{\lambda^*})(1 - \frac{I_n \lambda^*}{I_n^* \lambda}) + 3 - \frac{S_n^*}{S_n} - \frac{\lambda S_n E^*}{\lambda^* S_n^* E} - \frac{I_n \lambda^*}{I_n^* \lambda} - \frac{E}{E^*} + \frac{I_n}{I_n^*}\Big) \\
& \leq \Big(- (\frac{S_n^*}{S_n} - 1) - (\frac{\lambda S_n E^*}{\lambda^* S_n^* E} - 1) - (\frac{I_n \lambda^*}{I_n^* \lambda} - 1) - \frac{E}{E^*} + \frac{I_n}{I_n^*}\Big) \\
& \leq \Big(- \ln(\frac{S_n^*}{S_n} \frac{\lambda S_n E^*}{\lambda^* S_n^* E} \frac{I_n \lambda^*}{I_n^* \lambda}) - \frac{E}{E^*} + \frac{I_n}{I_n^*}\Big) \\
& = \Big(\frac{I_n}{I_n^*} - \ln(\frac{I_n}{I_n^*}) + \ln(\frac{E}{E^*}) - \frac{E}{E^*}\Big).
\end{aligned} \tag{A-10}$$

Similarly

$$\Big(2 - \frac{S_y^*}{S_y} - \frac{E}{E^*} - \frac{\lambda S_y E^*}{\lambda^* S_y^* E} + \frac{\lambda}{\lambda^*}\Big) \leq \Big(\frac{I_n}{I_n^*} - \ln(\frac{I_n}{I_n^*}) + \ln(\frac{E}{E^*}) - \frac{E}{E^*}\Big). \tag{A-11}$$

Also from Eq (A-7), we have

$$\begin{aligned}
\frac{E}{E^*} - \frac{I_n}{I_n^*} - \frac{I_n^* E}{I_n E^*} + 1 &= \Big(u\Big(\frac{I_n^* E}{I_n E^*}\Big) + \frac{E}{E^*} - \ln\Big(\frac{E}{E^*}\Big) - \frac{I_n}{I_n^*} + \ln\Big(\frac{I_n}{I_n^*}\Big)\Big) \\
&\leq \frac{E}{E^*} - \ln\Big(\frac{E}{E^*}\Big) + \ln\Big(\frac{I_n}{I_n^*}\Big) - \frac{I_n}{I_n^*}.
\end{aligned} \tag{A-12}$$

Similarly,

$$\frac{E}{E^*} + \frac{I_y}{I_y^*} - \frac{I_y^* E}{I_y E^*} + 1 \leq \frac{-I_y}{I_y^*} + \ln\left(\frac{I_y}{I_y^*}\right) + \ln\left(\frac{E}{E^*}\right) - \frac{E}{E^*}. \tag{A-13}$$

$$\frac{I_n}{I_n^*} + \frac{I_y}{I_y^*} - \frac{I_y^* I_n}{I_y I_n^*} + 1 \leq \frac{-I_y}{I_y^*} + \ln\left(\frac{I_y}{I_y^*}\right) + \ln\left(\frac{I_n}{I_n^*}\right) - \frac{I_n}{I_n^*}. \tag{A-14}$$

$$\frac{I_n}{I_n^*} + \frac{J}{J^*} - \frac{J^* I_n}{J I_n^*} + 1 \leq \frac{-J}{J^*} + \ln\left(\frac{J}{J^*}\right) + \ln\left(\frac{I_n}{I_n^*}\right) - \frac{I_n}{I_n^*}. \tag{A-15}$$

$$\frac{I_y}{I_y^*} + \frac{J}{J^*} - \frac{J^* I_y}{J I_y^*} + 1 \leq \frac{-J}{J^*} + \ln\left(\frac{J}{J^*}\right) + \ln\left(\frac{I_y}{I_y^*}\right) - \frac{I_y}{I_y^*}. \tag{A-16}$$

Hence,

$$\begin{aligned}
\dot{\mathfrak{I}}(t) \leq & \lambda^* S_n^* \left(\frac{I_n}{I_n^*} - \ln\left(\frac{I_n}{I_n^*}\right) + \ln\left(\frac{E}{E^*}\right) - \frac{E}{E^*}\right) + \\
& \epsilon\lambda^* S_y^* \left(\frac{I_n}{I_n^*} - \ln\left(\frac{I_n}{I_n^*}\right) + \ln\left(\frac{E}{E^*}\right) - \frac{E}{E^*}\right) + \\
& \lambda^* S_n^* \left(\frac{E}{E^*} - \ln\left(\frac{E}{E^*}\right) + \ln\left(\frac{I_n}{I_n^*}\right) - \frac{I_n}{I_n^*}\right) + \\
& \epsilon\lambda^* S_y^* \left(\frac{E}{E^*} - \ln\left(\frac{E}{E^*}\right) + \ln\left(\frac{I_n}{I_n^*}\right) - \frac{I_n}{I_n^*}\right) + \\
& \sigma_y E^* \left(\frac{-I_y}{I_y^*} + \ln\left(\frac{I_y}{I_y^*}\right) + \ln\left(\frac{E}{E^*}\right) - \frac{E}{E^*}\right) + \\
& \eta I_n^* \left(\frac{-I_y}{I_y^*} + \ln\left(\frac{I_y}{I_y^*}\right) + \ln\left(\frac{I_n}{I_n^*}\right) - \frac{I_n}{I_n^*}\right) + \\
& \gamma_n^* I_n^* \left(\frac{-J}{J^*} + \ln\left(\frac{J}{J^*}\right) + \ln\left(\frac{I_n}{I_n^*}\right) - \frac{I_n}{I_n^*}\right) + \\
& \gamma_y^* I_y^* \left(\frac{-J}{J^*} + \ln\left(\frac{J}{J^*}\right) + \ln\left(\frac{I_y}{I_y^*}\right) - \frac{I_y}{I_y^*}\right).
\end{aligned} \tag{A-17}$$

Equations (A-3)–(A-17) and conditions (i) $(1 - \frac{\lambda}{\lambda^*})(1 - \frac{I_n \lambda^*}{I_n^* \lambda}) \geq 0$, (ii) $\frac{I_y}{I_y^*} + \frac{E}{E^*} \geq \ln\left(\frac{I_y}{I_y^*}\right) + \ln\left(\frac{E}{E^*}\right)$, $\frac{I_y}{I_y^*} + \frac{I_n}{I_n^*} \geq \ln\left(\frac{I_y}{I_y^*}\right) + \ln\left(\frac{I_n}{I_n^*}\right)$, $\frac{J}{J^*} + \frac{I_n}{I_n^*} \geq \ln\left(\frac{J}{J^*}\right) + \ln\left(\frac{I_n}{I_n^*}\right)$, and $\frac{J}{J^*} + \frac{I_y}{I_y^*} \geq \ln\left(\frac{J}{J^*}\right) + \ln\left(\frac{I_y}{I_y^*}\right)$, ensure that $\dot{\mathfrak{I}}(t) \leq 0$. Further, the equality $\frac{d\mathfrak{I}}{dt} = 0$ holds only if $S_n = S_n^*$, $S_y = S_y^*$ $E = E^*$, $I_n = I_n^*$, $I_y = I_y^*$, and $J = J^*$. Thus, the EE state (B-1), is the only positive invariant set to the system (1) contained entirely in $\left\{(S_n, S_y, E, I_n, I_y, J) \in \Omega : S_n = S_n^*, S_y = S_y^*, E = E^*, I_n = I_n^*, I_y = I_y^*, J = J^*\right\}$. Hence, it follows from LaSalle's invariance principle [27] that every solution to the Eq (1) with initial conditions in Ω converge to EE points, Γ^*, as $t \to \infty$. Thus, the positive EE is globally asymptotically stable.

□

Appendix B: Bifurcation analysis

The bifurcation analysis is carried out using center manifold theory (CMT), as presented by Castillo-Chavez and Song [6]. The conditions for the parameter values in the model (1) that result in forward

or backward bifurcation are investigated. This approach has been widely used in earlier works, for example, [5, 6, 18, 31, 45]. When $\mathcal{R}_0$ crosses unity from below, there is a forward bifurcation, which results in the loss of stability of the DFE and the appearance of a small positive asymptotically stable equilibrium [6].

Theorem 5.1. *The mpoxv model* (1) *undergoes forward bifurcation at* $\mathcal{R}_0 = 1$ *whenever the bifurcation coefficients, A and B, are negative and positive, respectively.*

Proof. Following [5,6,30,45], we employ CMT. First, we let $\frac{dx}{dt} = f(x, \Xi)$, where Ξ is the bifurcation parameter, and f is continuously differentiable at least twice with respect to both x and Ξ. The DFE (Γ^0) is the point ($x_0 = 0, \Xi = 0$) and the local stability of Γ^0 changes at the point $(x_0, 0)$ [45]. We define a nontrivial equilibrium near the bifurcation point (x_0, Ξ).

Suppose that $\beta = \beta^*$ is chosen as a bifurcation parameter and we let $\mathcal{R}_0 = 1$ from (3). Then, by Theorem 5.1, the DFE Γ^0, is locally stable when $\beta < \beta^*$ and unstable when $\beta > \beta^*$. Here $\beta = \beta^*$ is a bifurcation value.

For convenience, let $S_n = x_1$, $S_y = x_2$, $E = x_3$, $I_n = x_4$, $I_y = x_5$, $J = x_6$ and $R = x_7$, so that $N = x_1+x_2+x_3+x_4+x_5+x_6+x_7$. Further, by adopting the same vector notation with $x = (x_1, x_2, ..., x_7)^T$, the model (1) can be written as $\frac{dx}{dt} = f(x)$ where $f = (f_1, f_2, ..., f_7)^T$ is as follows:

$$\begin{aligned}
f_1 &= (1-\rho)\pi - \lambda x_1 - A_5 x_1,\\
f_2 &= \pi\rho + \theta x_1 - \epsilon\lambda x_2 - \mu x_2,\\
f_3 &= \lambda(x_1 + \epsilon x_2) - A_1 x_3,\\
f_4 &= \sigma_n x_3 - A_2 x_4,\\
f_5 &= \sigma_y x_3 + \eta x_4 - A_3 x_5,\\
f_6 &= \gamma_n x_4 + \gamma_y x_5 - A_4 x_6,\\
f_7 &= \tau_n x_4 + \tau_y x_5 + \tau_J x_6 - \mu x_7,
\end{aligned} \tag{B-1}$$

where the associated forces of infection are respectively given by

$$\lambda = \frac{\beta(x_4 + \alpha x_5)}{\sum_{i=1}^{7} x_i}. \tag{B-2}$$

The Jacobian matrix of the system (B-2) (computed from the relation $J(\Gamma^0) = F - V$, where F and V are infection and transition matrices, respectively), evaluated at the DFE (Γ^0) with $\beta = \beta^*$, is given by

$$J(\Gamma^0) = \begin{bmatrix}
-A_0 & 0 & 0 & -c_1 & -c_4 & 0 & 0\\
\theta & -\mu & 0 & -c_2 & -c_5 & 0 & 0\\
0 & 0 & -A_1 & c_3 & c_6 & 0 & 0\\
0 & 0 & \sigma_n & -A_2 & 0 & 0 & 0\\
0 & 0 & \sigma_y & \eta & -A_3 & 0 & 0\\
0 & 0 & 0 & \gamma_n & \gamma_y & -A_4 & 0\\
0 & 0 & 0 & \tau_n & \tau_y & \tau_j & -\mu
\end{bmatrix}, \tag{B-3}$$

where
$c_1 = \frac{A_5\beta\mu}{\mu^3\rho+\theta(2\rho+1)\mu^2+\left((\rho+2)\theta^2+A_5\right)\mu+\theta^3}$, $c_2 = \frac{\epsilon(\mu\rho+\theta)(\theta+\mu)^2\beta}{\mu^3\rho+\theta(2\rho+1)\mu^2+\left((\rho+2)\theta^2+A_5\right)\mu+\theta^3}$,
$c_3 = \beta\left(\frac{\epsilon\pi(\mu\rho+\theta)(\theta+\mu)}{\mu}+\frac{\pi A_5}{\theta+\mu}\right)\left(\frac{\pi A_5}{\theta+\mu}+\frac{\pi(\mu\rho+\theta)(\theta+\mu)}{\mu}\right)^{-1}$, $c_4 = \frac{A_5\beta\alpha\mu}{\mu^3\rho+\theta(2\rho+1)\mu^2+\left((\rho+2)\theta^2+A_5\right)\mu+\theta^3}$,
$c_5 = \frac{\epsilon(\mu\rho+\theta)(\theta+\mu)^2\beta\alpha}{\mu^3\rho+\theta(2\rho+1)\mu^2+\left((\rho+2)\theta^2+A_5\right)\mu+\theta^3}$, and $c_6 = \beta\alpha\left(\frac{\epsilon\pi(\mu\rho+\theta)(\theta+\mu)}{\mu}+\frac{\pi A_5}{\theta+\mu}\right)\left(\frac{\pi A_5}{\theta+\mu}+\frac{\pi(\mu\rho+\theta)(\theta+\mu)}{\mu}\right)^{-1}$.

The Jacobian matrix $J(\Gamma^0)$ of the system (B-2) has a simple zero eigenvalue (other eigenvalues have negative real parts). Hence, the CMT [6, 45] can be employed to analyse the dynamics of the system (B-2) located at $\beta = \beta^*$ [6]. The subsequent computations are carried out using similar notations as in [6].

Eigenvectors of $J(\Gamma^0)_{\beta=\beta^*}$: For the case when $\mathcal{R}_0 = 1$, it can be shown that the $J(\Gamma^0)$ has a right eigenvector (corresponding to the zero eigenvalues), given by $\Psi = (\Psi_1, \Psi_2, ..., \Psi_7)^T$, where

$$\begin{aligned}
\Psi_1 &= \frac{A_3c_1\sigma_n + c_5A_2\sigma_y + n_5\eta\sigma_n}{A_0A_2A_3}\Psi_3,\\
\Psi_2 &= \frac{\theta A_3c_1\sigma_n + \theta c_5A_2\sigma_y + \theta c_5\eta\sigma_n + A_0A_3c_2\sigma_n + A_0c_5A_2\sigma_y + A_0c_5\eta\sigma_n}{\mu A_0A_2A_3}\Psi_3,\\
\Psi_3 &> 0,\\
\Psi_4 &= \frac{\sigma_n}{A_2}\Psi_3,\\
\Psi_5 &= \frac{A_2\sigma_y + \eta\sigma_n}{A_2A_3}\Psi_3,\\
\Psi_6 &= \frac{A_3\gamma_n\sigma_n + \gamma_yA_2\sigma_y + \gamma_y\eta\sigma_n}{A_2A_3A_4}\Psi_3,\\
\Psi_7 &= \frac{A_3A_4\tau_n\sigma_n + A_4\tau_yA_2\sigma_y + A_4\tau_y\eta\sigma_n + \tau_JA_3\gamma_n\sigma_n + \tau_J\gamma_yA_2\sigma_y + \tau_J\gamma_y\eta\sigma_n}{\mu A_2A_3A_4}\Psi_3.
\end{aligned} \tag{B-4}$$

Similarly, the components of the left eigenvector of $J(\Gamma^0)$ (corresponding to the zero eigenvalue), denoted by $\Phi = (\Phi_1, \Phi_2, ..., \Phi_7)$, are given by

$$\begin{aligned}
\Phi_1 &= 0,\\
\Phi_2 &= 0,\\
\Phi_3 &> 0,\\
\Phi_4 &= \frac{c_3(\sigma_n\eta - A_2\sigma_y) - \eta(\sigma_nc_3 - A_1A_2)}{A_2(\sigma_n\eta - A_2\sigma_y)}\Phi_3,\\
\Phi_5 &= \frac{(\sigma_nc_3 - A_1A_2)}{\sigma_n\eta - A_2\sigma_y}\Phi_3,\\
\Phi_6 &= 0,\\
\Phi_7 &= 0.
\end{aligned} \tag{B-5}$$

Note that the free components (entry) are chosen to be $\Phi_3 = 1$ and $\Psi_3 = \frac{1}{A_1+A_2}$ respectively, where

$$A_1 = 1 + \frac{\sigma_n}{A_2} + \left(\frac{c_3(\sigma_n\eta - A_2\sigma_y) - \eta(\sigma_nc_3 - A_1A_2)}{A_2(\sigma_n\eta - A_2\sigma_y)}\right) \quad \text{and} \quad A_2 = \frac{\sigma_nc_3 - A_1A_2}{\sigma_n\eta - A_2\sigma_y}\frac{A_2\sigma_y + \eta\sigma_n}{A_2A_3}, \tag{B-6}$$

so that, $\mathbf{v} \cdot \mathbf{w} = 1$ (in line with [6]).

It can be shown, by computing the non-zero partial derivatives of f_i ($i = 1, ..., 7$), that the associated bifurcation coefficients, A and B, are given, respectively, by

$$\begin{aligned} A &= \sum_{k,i,j=1}^{7} \Phi_k \Psi_i \Psi_j \frac{\partial^2 f_k(0,0)}{\partial x_i \partial x_j} \\ &= -2A_0 \frac{[\rho U_1 \mu^3 + 2U_1(\rho + \frac{1}{2})\theta\mu^2 + ((\rho+2)U_1\theta^2 - A_5U_2)\mu + U_1\theta^3](\alpha\Psi_5 + \Psi_4)\mu\beta\Phi_3}{\pi\left(\mu^3\rho + \theta\left(2\rho+1\right)\mu^2 + \left(\left(\rho+2\right)\theta^2 + A_5\right)\mu + \theta^3\right)^2}, \end{aligned} \tag{B-7}$$

$$B = \sum_{k,i=1}^{7} \Phi_k \Psi_i \frac{\partial^2 f_k(0,0)}{\partial x_i \partial \beta} = \frac{(\Psi_4 + \alpha\,\Psi_5)\left(\epsilon\,\mu^3\rho + 2\,\epsilon\,\mu^2\rho\,\theta + \epsilon\,\mu\,\rho\,\theta^2 + \epsilon\,\mu^2\theta + 2\,\epsilon\,\mu\,\theta^2 + \epsilon\,\theta^3 + \mu\,A_5\right)\Phi_3}{\mu^3\rho + 2\,\mu^2\rho\,\theta + \mu\,\rho\,\theta^2 + \mu^2\theta + 2\,\mu\,\theta^2 + \theta^3 + \mu\,A_5}, \tag{B-8}$$

where $U_1 = (\Psi_1 + \Psi_3 + \Psi_4 + \Psi_5 + \Psi_6 + \Psi_7)\epsilon - \Psi_1$ and $U_2 = \epsilon\Psi_2 - \Psi_2 - \Psi_3 - \Psi_4 - \Psi_5 - \Psi_6 - \Psi_7$. Now, since $\Phi_3 > 0$, $\Psi_3 > 0$, $\Psi_4 > 0$, and $\Psi_5 > 0$, indicating that $B \geq 0$, therefore, forward bifurcation occurs if and only if $A < 0$ else we have backward bifurcation (i.e. when $A > 0$). To verify the above results numerically, we computed the expression using the parameter values in Table 2 and found that A (-651.5562000) and B (5.585740031) were negative and positive, respectively. As a result, forward bifurcation is likely for the mpoxv model (1) at $\mathcal{R}_0 = 1$. Furthermore, an EE will not exist if $\mathcal{R}_0 < 1$, leaving DFE as the only local attractor. However, if $\mathcal{R}_0 > 1$, the EE exists. Therefore, a forward bifurcation likely exists because disease prevalence is an increasing function of $\mathcal{R}_0$ in the vicinity of the bifurcation point.

□